Journal of Sustainability Science and Management
Volume 16 Number 8, December 2021: 158-176
eISSN: 2672-7226

A PRELIMINARY STUDY: MOLECULAR DOCKING, OPTIMIZATION AND CHARACTERIZATION OF KOJIC MONOOLEATE NANOEMULSION FOR COSMECEUTICALS APPLICATION

ROSELAN MUHAMMAD AZIMUDDIN[1,2], ZAKARIA NORZALINA[1,2], FAUJAN NUR HANA[1,2,3]*, SYED AZHAR SHARIFAH NURFADHLIN AFIFAH[1,2] AND SITI EFLIZA ASHARI[1,2,3]*

[1]Department of Chemistry, Faculty of Science, Universiti Putra Malaysia, Serdang 43400, Selangor, Malaysia. [2]Integrated Chemical BioPhysics Research, Faculty of Science, Universiti Putra Malaysia, Serdang 43400, Selangor, Malaysia. [3]Centre of Foundation Studies for Agricultural Sciences, Universiti Putra Malaysia, Serdang 43400, Selangor, Malaysia.

**Corresponding author: nurhana@upm.edu.my and ctefliza@upm.edu.my*
Submitted final draft: 7 January 2021 *Accepted: 18 February 2021* http://doi.org/10.46754/jssm.2021.12.011

Abstract: Skin hyperpigmentation disease occurs when there is an abnormal production of melanin synthesized in the melanocyte. One of the kojic acid derivatives, namely kojic monooleate, has shown better depigmenting effect than KA. In this study, molecular docking simulation was conducted to predict the binding mechanism of KMO against tyrosinase enzymes prior to the preliminary study of the process parameters in the production of KMO nanoemulsion using response surface methodology. The binding affinity for the best-bound mode of KMO against mushroom (PDB ID: 2Y9W) and human (PDB ID: 5M8M) tyrosinase enzymes were -4.0 kcal/mol and -5.1 kcal/mol, respectively. The optimized conditions for the formulation of KMO nanoemulsion was 11.16 min (time of high shear), 218.32 rpm (speed of low shear), and 16.75 min (sonication time) that resulted in 220.41 nm of particle size. The pH and conductivity of the KMO nanoemulsion were found to be 4.76 and 1405 µS/cm, respectively, and it remains stable under centrifugation test and different storage temperatures. The data from this study can be used to provide additional information on the capability of KMO as an antityrosinase in further development of KMO nanoemulsion with desirable criteria for cosmeceuticals applications.

Keywords: Nanoemulsion, kojic monooleate, molecular docking, hyperpigmentation, response surface methodology, optimization, tyrosinase.

Introduction

Tyrosinase has been considered an important enzyme for the development of therapeutic agents to solve hyperpigmentation diseases in the cosmeceutical field. In humans, tyrosinase is involved in the biosynthesis of melanin, which is a skin pigment, derived from tyrosine during the melanogenesis process that will determine the color of mammalian skin, eyes and hair (Huang *et al*., 2008; Bahari *et al*., 2020). Abnormal production of melanin will result in various skin disorders, such as hyperpigmentation, melisma, malign melanoma, and skin-aging processes (Heo *et al*., 2010; Panich *et al.*, 2010). This abnormal production may be caused by several factors, such as UV radiation, radicals, inflammatory mediators, and hormones (Kanlayavattanakul & Lourith, 2018). Thus, if tyrosinase can be inhibited, it will significantly alter the production of the melanin.

Kojic Acid (KA) is one of the most used skin whitening agents. It is an antibiotic produced by many species of *Aspergillus*, *Acetobactor* and *Penicillum* through an aerobic process (Jumbri *et al*., 2015). However, KA was described as a less stable compound (Noh *et al*., 2009; Jumbri *et al*., 2015), due to its sensitivity to light and heat (Gallarate *et al*., 2004). The effectiveness of this compound as a whitening agent will be reduced when exposed under sun or air. Kojic Monooleate (KMO), which is a palm-based fatty acid derivative of KA was found to have a significant effect in tyrosinase inhibition compared to kojic monolaurate and kojic monopalmitate (Syed Azhar *et al*., 2018). This shows that KA esters, specifically KMO,

can be used as one of the skin whitening agents to inhibit tyrosinase to treat hyperpigmentation.

The binding mechanism of the KMO against tyrosinase enzymes can be predicted by utilizing molecular docking approach. Molecular docking is a computational method that aims to predict the favoured orientation of a ligand to its target protein and calculates the binding affinity, binding mode as well as binding residues of a protein-ligand complex. In other words, molecular docking was performed in this study to understand the interaction between KMO (ligand) and tyrosinase (protein). This method can be used to provide helpful data for proposing effective tyrosinase inhibitors.

The major concern for the development of cosmeceutical products to treat hyperpigmentation disease is the effectiveness of the delivery system to deliver the active ingredients to its targeted site. Nanotechnology-based innovations, such as nanoemulsions, nano-capsules, nano-pigments and liposomes, are widely used in various types of cosmetic products (Lohani *et al.*, 2014). Emulsions are made up of two immiscible fluids, where one fluid is dispersed into another fluid with the presence of a surfactant to lower the surface tension between these two fluids. Meanwhile, nanoemulsions are defined as emulsion systems having particle sizes ranging from 20 - 500 nm (Pey *et al*., 2006; Solè *et al*., 2006). Due to their very fine particle size, nanoemulsions possess excellent stability against sedimentation and can deliver active ingredients efficiently, as it has a larger surface area for rapid penetrations and enhances penetration through the rough skin (Tadros *et al.*, 2004). Nanoemulsions are not only being used in cosmeceuticals, but its spherical shape and group of dispersed droplets are also being used in foods, chemical and pesticide industries (Sharma *et al*., 2010; McClements, 2011; Abdellatif & Abou-Taleb, 2015). To date, nanoemulsions have been a popular delivery system for the development of cosmeceuticals products to treat hyperpigmentation (Al-Edresi & Baie, 2009; Jacobus Berlitz *et al*., 2019; Tofani *et al*., 2016).

This study aims to predict the binding mechanism of the KMO against human (PDB ID: 5M8M) and mushroom (2Y9W) tyrosinase enzymes. Following the verification of the binding mechanism of KMO against tyrosinase enzymes, the KMO was then loaded into a nanoemulsion system. The preliminary optimization by utilizing response surface methodology (RSM) was performed to determine the optimum processing parameters in the production of KMO nanoemulsion with the desirable particle size and physicochemical properties.

Materials and Methods

Materials

KMO was synthesized according to the method used by Jumbri *et al.* (2015). Tween 80 was purchased from Merck Chemicals (Darmstadt, Germany). Castor oil and xanthan gum (from *Xanthomonas campestris*) were purchased from Sigma-Aldrich (St. Louis, MO, USA). South African lemon essential oil was purchased from Wellness Original Ingredient (Puchong, Malaysia). Phenonip was purchased from Bramble Berry (WA, USA). Deionized water was purified using a Milli-Q water system (EMD Millipore, Billerica, MA, USA). Chemicals used were all analytical, food or cosmetic grade.

Molecular Docking

The molecular docking was conducted to predict the binding structures of human (PDB ID: 5M8M) and mushroom (PDB ID: 2Y9W) tyrosinase with KMO and KA. Prior to molecular docking, the validation study was done using co-crystallised KA (retrieved from 5M8M complex) to validate the docking parameters. For ligand comparison analysis, the structure of KMO (PubChem CID: 100926368) from PubChem was also docked with 5M8M protein.

Preparation of Protein

The crystal structure of tyrosinase proteins (PDB ID: 5M8M and 2Y9W) were obtained

from Protein Data Bank (http://www.rcsb.org). The human tyrosinase (PDB ID: 5M8M) contains three zinc (II) ions in the active site instead of copper (II) ions as found in common tyrosinase, which explains why this enzyme did not exhibit tyrosinase redox activity (Lai *et al*., 2017). Human tyrosinase contains four conserved regions; an N-terminal signal peptide, an intramelanosomal domain, a single transmembrane alpha helix, and a small, flexible C-terminal cytoplasmic domain (Lai *et al*., 2017). The tyrosinase derived from mushroom *Agaricus bisporus* (PDB ID: 2Y9W) is commonly found as a H_2L_2 tetramer. The H subunit contains two copper atoms coordinated by six histidine (His85, His61, His94, His259, His263 and His296) residues, and the L subunit consist of a lectin-like fold (Ismaya *et al*., 2011). The water molecules and all ligands (KA) were discarded, and co-crystallised ligands, including water molecules and holmium ions, were removed from the target enzyme, except copper (II) and zinc (II) ions. Autodock Tools (ADT) does not provide any charges for metal ions. Thus, the manual addition of charges was done in the PDBQT file using a text editor (Forli *et al*., 2016). Finally, polar hydrogens were added to the protein using AutoDockTools 4.2 (The Scripps Research Institute, La Jolla, CA, USA) (Sanner, 1999).

Preparation of Ligand

The two-dimensional (2D) structure of KMO was obtained from http://pubchem.ncbi.nlm.nih.gov/ (PubChem ID: 100926368) in SDF format and converted into PDB structure using Discovery Studio Visualizer 19.1 (Dassault Systems Biovia, San Diego, CA, USA). The three-dimensional (3D) structure of co-crystallised KA compound was extracted from 5M8M also using Discovery Studio Visualizer 19.1.

Docking Procedure

To investigate the binding interactions of KA and KMO to tyrosinase enzymes, AutoDock Vina 1.1.2 (The Scripps Research Institute, La Jolla, CA, USA) (Trott & Olson, 2009) software package was utilized. All water molecules, nonpolar hydrogen atoms and ligands were removed before re-docking, only leaving behind the Chain A of TYRP1. The grid box was set to 112 Å x 126 Å x 126 Å with a center grid of -35.634, 8.151 and -23.501 in X, Y and Z dimensions to cover all amino acid residues of Chain A. The grid and docking parameter files were prepared using AutoDockTools 4.2 (The Scripps Research Institute, La Jolla, CA, USA) (Sanner, 1999). The docked pose and crystallised structure of KA were superimposed and its root mean square deviation (RMSD) was calculated using AutoDockTools 4.2 (The Scripps Research Institute, La Jolla, CA, USA) (Sanner, 1999). The interacting amino acid residues were visualized using Discovery Studio Visualizer 19.1 (Dassault Systems Biovia, San Diego, CA, USA).

After validation of the docking protocol, the 3D structure of co-crystallised KA and KMO were docked into the tyrosinase enzymes. All parameters in the control docking were applied to dock the co-crystallised KA and KMO against tyrosinase enzymes. The protein was kept rigid while the ligand was kept flexible during the docking process (Damayanti *et al*., 2014). The binding affinity of the resulting docking pose was then determined using AutoDock Vina 1.1.2 (Trott & Olson, 2009). The interaction energy between the ligand and the receptor was then calculated and expressed as affinity (kcal/mol). The best-docked poses from the docking results were analyzed using AutoDockTools 4.2 (The Scripps Research Institute, La Jolla, CA, USA) (Sanner, 1999) and Discovery Studio Visualizer 19.1 (Dassault Systems Biovia, San Diego, CA, USA). The identification of the active site was analyzed from the literature using CASTp (Dundas *et al*., 2006) tools.

Preparation of KMO Nanoemulsion

For the preparation of KMO nanoemulsion, two phases of developing nanoemulsions were prepared; oil phase and aqueous phase. The oil phase was obtained by blending 10% w/w of

KMO and 2.7% w/w of castor oil, while for the aqueous phase, 4% w/w of tween 80 and 1.5% w/w of xanthan gum was added to 80.8% w/w of deionized water. Each phase was heated separately up to 30°C while being stirred using a magnetic stirrer to ensure the formation of a homogenous solution before sonicated using an ultrasonic bath sonicator (Power Sonic 405, Hwashin Technology Co., Seoul, Korea). The oil phase was gradually added dropwise into the aqueous phase while being homogenized using a high shear homogenizer (T25 digital; IKA-Werk, GmbH & Co. KG, Staufen im Breisgau, Germany) at 6000 rpm. Finally, the mixture was further homogenized using an overhead stirrer (RW20 digital; IKA-Werk) for 3 h while adding 0.3% w/w of lemon oil and 0.7% w/w of phenonip. The lemon oil was used to give a pleasant fragrance in the nanoemulsion. Furthermore, lemon oil was found to be able to ease stress and elevate mood (Fukumoto *et al*., 2008). Meanwhile, phenonip was used as a preservative, to protect the nanoemulsion from microbial insults which may occur from raw materials, manufacturing and consumer use (Nostro *et al*., 2004).

Experimental Design

A three-factors-five-level central composite design (CCD) was employed in the preliminary determination of the optimum processing conditions, which include time of high shear (A), speed of low shear (B), and sonication time (C) towards the particle size of the nanoemulsion as its response. The speed of high shear and time of low shear were kept constant at 6000 rpm and 3 hours, respectively. A summary of the independent variables and their coded levels are tabulated in Table 1.

The design matrix was developed using Design-Expert® software (version 7.1.5; Stat Ease Inc., Minneopolis, MN, USA). A total of 20 runs was developed, and the results were statistically evaluated. Three independent variables were run at five levels for each of the individual variables. Therefore, this design involves eight factorial points, six axial points, and six replicates of the center points. The effects of each variable and the interactions between variables on the outcomes can be studied independently using CCD (Tan *et al.*, 2016). The experiments were conducted at random to minimize the influence of the extraneous factor.

Statistical Analysis

Upon the completion of all runs, the analysis of variance (ANOVA) and coefficient of determination (R^2) was determined to study the significant differences among the independent variables in terms of a lack-of-fit test. The significance of the equation parameters for each response can be achieved with a probability value (p-value) less than 0.05 ($p < 0.05$). In this study, the optimum levels of the processing conditions (the time of high shear, the speed of low shear, and the sonication time) were determined to produce a nanoemulsion with desirable responses.

Verification of Model

The verification of the final model was carried out in terms of a validation set to study the adequacy of the predicted response value. Random formulations with different conditions were considered to validate the model. The

Table 1: Summary of independent variables and their coded levels

Independent Variables	Unit	Coded Level				
		-2	-1	0	+1	+2
A	min	5.00	8.04	12.50	16.96	20.00
B	rpm	4500.00	4905.40	5500.00	6094.60	6500.00
C	min	200.00	220.27	250.00	279.73	300.00

A = time of high shear; B = speed of low shear; C = sonication time

actual and predicted response values were used to calculate the percentage of residual standard error (Equation 1). The final optimum conditions suggested were also used to confirm the predicted optimum values of the model.

$$\text{Residual standard error (RSE)} = \frac{Actual\ value - Predicted\ value}{Predicted\ value} \quad (1)$$

Physicochemical Characterization of KMO Nanoemulsion

Particle Size, Zeta Potential and Polydispersity Index (PDI) Determination

The particle size, zeta potential and polydispersity index (PDI) of the nanoemulsion system were measured using dynamic light scattering, which scattered at an angle of 173° and a temperature of 25°C. This process was carried out using a particle size analyzer (Zetasizer Nano ZS90; Malvern Instruments, Malvern, UK). The measurement of particle size was done a day after the formulations were made to ensure that the system has achieved equilibrium (Baş & Boyacı, 2007). Deionized water was used to reduce the concentration of samples in order to avoid multiple scattering effects, before being filled into a folded capillary cell (DTS1070; Malvern Instruments). The count rate was maintained between 100 and 300 kcps. The measurement was repeated at least three times and the value was reported as mean value.

pH Measurement

The pH of the KMO nanoemulsion was determined using a Delta 320 pH meter (Mettler Toledo, Columbus, OH, USA). An electrode with a glass membrane that is sensitive to hydrogen ions was used to measure the pH value. Prior to taking measurements, the pH meter was calibrated with three standard buffer solutions (pH 4.00, 7.00 and 10.00). The pH value was determined by the direct insertion of the electrode into the sample. pH measurement is crucial to ensure that the KMO nanoemulsion is compatible with human skin.

Conductivity Measurement

Conductivity refers to the measurement of the free amount of water and ions. Conductivity measurements can be used to determine whether the KMO nanoemulsion formed is oil-in-water (O/W) or water-in-oil (W/O) nanoemulsion. The conductivity of the nanoemulsion containing KMO was determined using a conductometer (Mettler Toledo). The electrode was inserted directly into the sample before the conductivity value was measured.

Stability Study

The stability of nanoemulsion is defined by the capability of the formulation (in a specific system) to maintain its physical appearance, without any phase separation or physical changes over a specific time of storage and during use. The KMO nanoemulsion was subjected to two stability studies; stability under a centrifugation test and storage stability at different temperatures (4°C, 25°C and 45°C) for 90 days. The stability of the KMO nanoemulsion was determined through the visible appearance of creaming or phase separation.

To test its stability under a centrifugation test, the KMO nanoemulsion was kept in a centrifuge tube and was subjected to centrifugation force (EBA 200; Hettich Zentrifugen, Tuttlingen, Germany) at 4000 rpm for 15 minutes. The KMO nanoemulsion was then observed for any phase separation or physical change.

To determine its storage stability at different temperatures, the KMO nanoemulsion was observed in terms of its physical appearance on days 1, 30, 60 and 90 of storage time.

Results and Discussion

Molecular Docking

The molecular docking simulation was conducted to clarify the molecular mechanism of KMO against human (PDB ID: 5M8M) and mushroom (PDB ID: 2Y9W) tyrosinase enzymes by utilizing AutoDock Vina 1.1.2 (Trott & Olson, 2009) software. To assess the accuracy

of the computational docking protocol, control docking was performed by re-docking of co-crystallised KA against human tyrosinase (PDB ID: 5M8M) (Ibrahim *et al*., 2016). Then, its root mean square deviation (RMSD) relative to its crystallographic orientation was measured. The RMSD value of 2.0 Å or less was considered an acceptable pose which indicates the success of docking (Makeneni *et al*., 2018). The docking conformation of KA with the lowest binding affinity was compared with the crystal structure of KA based on its RMSD value, which was 2.074 Å. This value is acceptable as it only exceeded the threshold limit by 0.74 Å.

After the docking protocol has been validated, the 3D structure of KMO was docked into tyrosinase enzymes. Table 2 shows the binding affinities of the docked position and the favorable interactions with the key amino acid residues of co-crystallised KA (PDB ID: 5M8M) and KMO (PubChem CID: 100926368) ligand compounds with tyrosinase (PDB ID: 5M8M and 2Y9W) enzymes. The ligand binding affinity is defined by the binding energy of ligand to the receptor which is influenced by non-covalent intermolecular interaction such as hydrogen bonding, hydrophobic, electrostatic interactions and van der Waals forces between the two molecules (Faujan *et al*., 2019).

In this study, the results demonstrate some variation of affinity value, where the values obtained ranged from -5.6 to -4.0 kcal/mol, as shown in Table 2. The strongest binding affinity value was found to be for KA-5M8M complex (-5.6 kcal/mol), followed by the KMO-2Y9W, KA-2Y9W, and KMO-5M8M complexes. The best docking pose was also identified to reveal the most interacting residues in the active sites of human (PDB ID: 5M8M) and mushroom (PDB ID: 2Y9W) tyrosinase. The interactions between co-crystallised KA and KMO against both tyrosinase enzymes are shown in Figure 1.

Table 2: Binding affinity and amino acid interactions of co-crystallized KA and KMO against tyrosinase enzymes

Ligand	Tyrosinase	Affinity (kcal/mol)	Binding Interaction	Amino Acid Residue
KA	5M8M	-5.6	H-bond	Ser394
			Van der Waal	His192, His215, His224, His 377, Asn378, Leu382, Gly388, Gly389, Gln390, Thr391, Phe400
			Pi-interactions	His381 (π-π stacked)
	2Y9W	-4.5	H-bond	Ser2, Glu67, Gln74
			Van der Waal	Asp3, Lys4, Lys70, Gln72, Pro73
			Pi-interactions	Lys5 (π-cation)
KMO	5M8M	-4.0	H-bond	Ser183, Asn186
			Van der Waal	Lys152, Arg153, Thr155, Glu180, Asn181, Ile182, Ser305
			Pi-interactions	-
	2Y9W	-5.1	H-bond	Asn174, Lys180
			Van der Waal	Gln41, Gln44, Lys158, Ile170, Glu171, Val172, Glu173, Pro175, Leu177, His178, Tyr179
			Pi-interactions	Lys180 (π-alkyl)

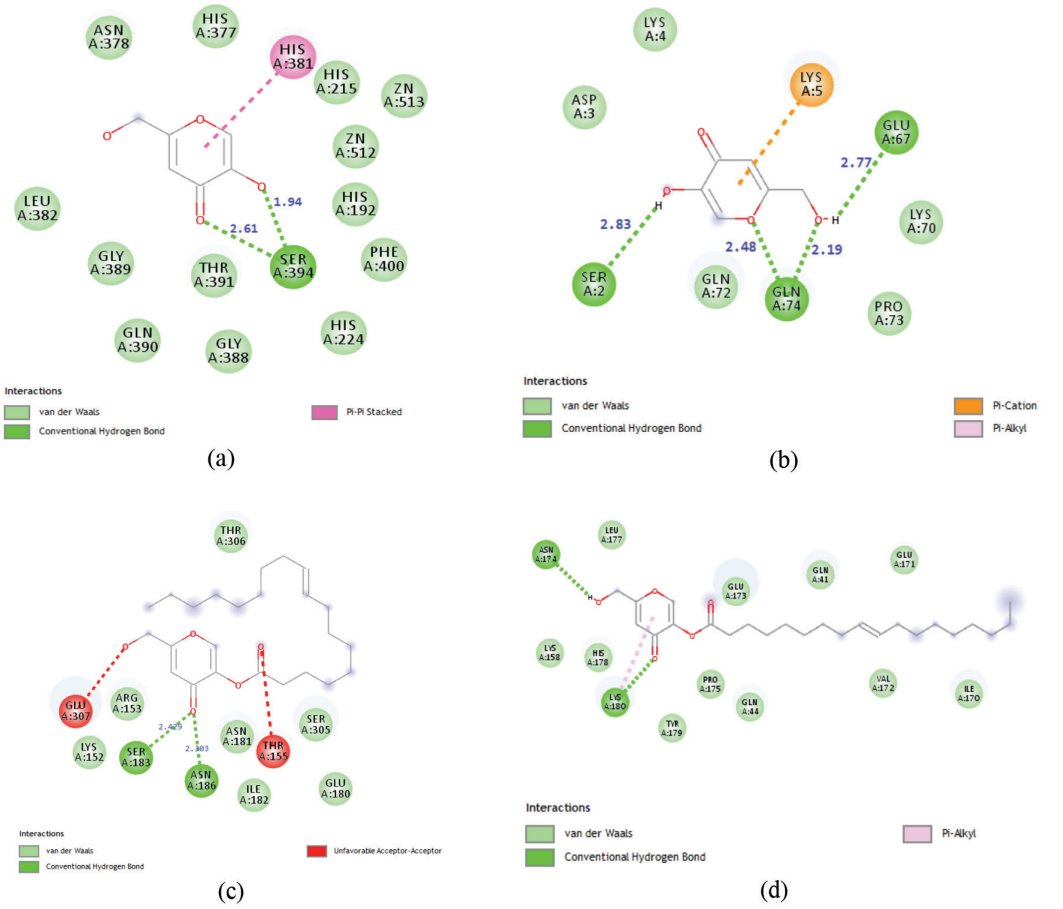

Figure 1: The interactions between co-crystallised KA with (a) 5M8M and (b) 2Y9W tyrosinase, and KMO with (c) 5M8M and (d) 2Y9W tyrosinase

As shown in Figure 1(a) and Figure 1(b), the co-crystallised KA binds differently in both tyrosinase enzymes, where two hydrogen bonds formed against 5M8M, along with four hydrogen bonds against 2Y9W receptors. In the crystal structure of the 5M8M docked complex, co-crystallised KA makes hydrogen bonds with Ser394 between the oxygen atom of the hydroxyl and oxo groups at distance 1.937 Å and 2.615 Å, respectively. The specific hydrogen bonding interaction was found in the docked conformation of mushroom tyrosinase (PDB ID: 2Y9W); one hydrogen bond between ring oxygen atom with Gln74 (2.476 Å), two hydrogen bonds exist between the hydroxymethyl group of co-crystallised KA with Gln74 (2.187 Å) and Glu67 (2.775 Å), and a hydrogen bond between hydroxyl group with Ser2 (2.829 Å).

The most van der Waals interaction of co-crystallised KA was found in the 5M8M docked complex, followed by 2Y9W docked complexes. The co-crystallised KA interacted with His192, His215, His224, His377, Asn378, Leu382, Gly388, Gly389, Gln390, Thr391 and Phe400 residues through the van der Waals interactions. As shown in Figure 1, the co-crystallised KA interacted via π-π stacked with His381 in 5M8M docked complex. The docked conformation revealed that co-crystallised KA was able to interact with zinc ions by His215 and His192 in the 5M8M docked complex. The co-

crystalized KA does not interact with histidine in the 2Y9W docked complex. However, van der Waals interactions with Asp3, Lys4, Lys70, Gln72 and Pro73 as well as π-cation with Lys5 were detected in the 2Y9W docked complex.

As for KMO, two hydrogen bonds were formed against 5M8M tyrosinase between the oxo group with Ser183 (2.429 Å) and Asn186 (2.303 Å), respectively, as shown in Figure 1(c). The specific hydrogen bonding interaction between oxo groups was also found in 2Y9W receptors with Thr306 and Lys180 residues at distances 2.795 Å and 2.234 Å, respectively [Figure 1(d)]. Additionally, hydrogen bonding interactions exist between the hydrogen atom of the hydroxymethyl group of KMO with Glu307, Met238 and Asn174 in the 2Y9W receptors. In the case of the KMO compound, the molecule does not make any interactions with the hydroxyl group and the oxygen atom of the hydroxymethyl group. Interestingly, the KMO molecule forms more hydrogen bonding interactions against 2Y9W compared with KA.

In Figure 1(c), van der Waals interactions between KMO and Lys152, Arg153, Thr155, Glu180, Asn181, Ile182 and Ser305 were observed in the 5M8M docked complex. In 2Y9W docked complex [Figure 1(d)], KMO shows the most favorable van der Waals interactions as compared with co-crystallised KA, where the KMO interacted with Gln41, Gln44, Lys158, Ile170, Glu171, Val172, Glu173, Pro175, Leu177, His178 and Tyr179. The KMO also interacted with Lys180 via π-alkyl interaction.

Fitting the Model

The mean particle size of the KMO nanoemulsion obtained experimentally, according to CCD is tabulated in Table 3.

Table 3 shows that the minimum particle size obtained experimentally was 184.60 nm (run no. 5). Some of the actual particle size values were in good agreement with the predicted values, and others have largely deviated from the predicted values. The final equation to predict the particle size in terms of coded factors for the second-order polynomial is shown in Equation **2: $Y = 302.24 + 95.69A + 8.12B - 94.18C - 2.69AB + 20.46AC - 13.03BC + 34.11A^2 + 115.71B^2 + 50.50C^2$ (2)**

where A, B, and C represent the values of the time of high shear, the speed of low shear, and the sonication time, respectively. Figure 2 shows the scatter plot of predicted particle size versus actual particle size values from CCD.

The predicted particle size values derived from the model versus the actual particle size values obtained from the experimental data show that the model was successful in capturing the correlation between all the independent variables, with R^2 = 0.8762 (Figure 2). This model shows an acceptable correlation between the experimental and predicted values. This is because few points are far away from the diagonal line.

ANOVA results for the effects of all independent variables were implemented using Design-Expert® software (version 7.1.5) to investigate the suitability and also the significance of the final model, and it is presented in Table 4.

The *p*-value determines the significance of the model generated. The model was deemed insignificant if the *p*-value is greater than 0.1000, meanwhile, if the *p*-value is less than 0.0500, the model was deemed to be significant (Mohd *et al*., 2020). The final model was found to be significant with a small *p*-value (0.0017), a large *F*-value (7.87), and the lack of fit was not significant in the terms of the response (particle size). The *p*-value of the time of high shear (A) and the sonication time (C) were 0.0015 and 0.0017, respectively, indicating that both terms were significant. The terms (B^2 and C^2) and were also significant. Meanwhile, the speed of low shear (B) has no significant effect, with a *p*-value of 0.7209. This finding in the preliminary study can be used to further optimize the processing parameters in the production of the KMO nanoemulsion.

Table 3: Actual and predicted values of the particle size of the KMO nanoemulsion

Standard Order	Run Order	Independent Variables			Particle Size (nm)	
		Time of High Shear (min)	Speed of Low Shear (rpm)	Sonication Time (min)	Actual	Predicted
1	10	10.07	180.40	8.04	469.60	497.66
2	9	24.93	180.40	8.04	628.05	653.51
3	7	10.07	269.60	8.04	511.10	545.35
4	11	24.93	269.60	8.04	727.70	690.43
5	2	10.07	180.40	16.96	264.90	294.44
6	20	24.93	180.40	16.96	574.10	532.12
7	14	10.07	269.60	16.96	269.20	290.01
8	8	24.93	269.60	16.96	552.70	516.92
9	1	5.00	225.00	12.50	308.50	237.79
10	17	30.00	225.00	12.50	478.00	559.64
11	6	17.50	150.00	12.50	611.90	615.86
12	18	17.50	300.00	12.50	636.20	643.17
13	13	17.50	225.00	5.00	605.10	603.46
14	4	17.50	225.00	20.00	274.10	286.67
15	16	17.50	225.00	12.50	186.60	302.24
16	5	17.50	225.00	12.50	184.60	302.24
17	19	17.50	225.00	12.50	378.80	302.24
18	12	17.50	225.00	12.50	356.70	302.24
19	3	17.50	225.00	12.50	305.10	302.24
20	15	17.50	225.00	12.50	403.50	302.24

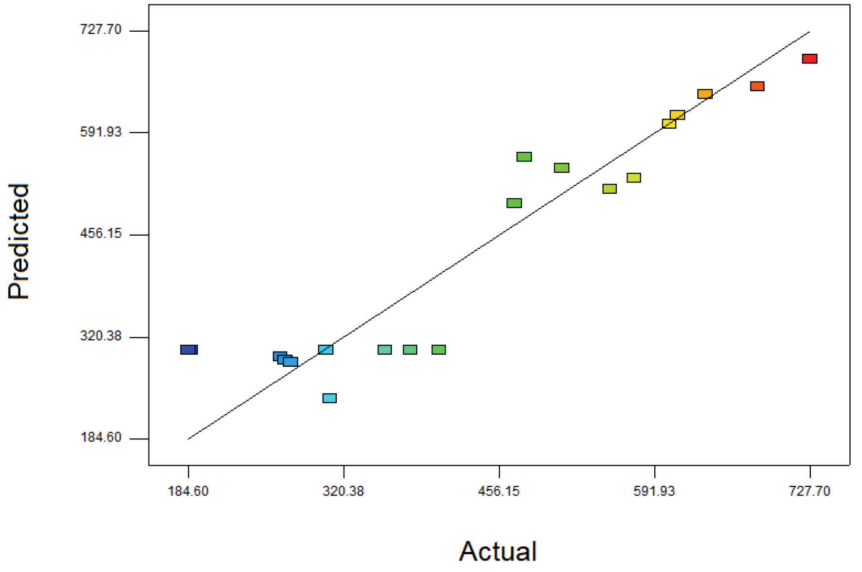

Figure 2: Scatter plot of predicted particle size versus actual particle size values from Central Composite Design (CCD)

Table 4: ANOVA results for the effect of all independent variables

Source	Sum of Squares	df	Mean Square	*F*-value	*p*-value	Significant
Model	4.723×10^5	9	52477.79	7.87	0.0017	significant
A	1.25×10^5	1	1.25×10^5	18.75	0.0015	
B	900.84	1	900.84	0.14	0.7209	
C	1.211×10^5	1	1.211×10^5	18.16	0.0017	
AB	58.05	1	58.05	8.703×10^{-3}	0.9275	
AC	3347.67	1	3347.67	0.50	0.4949	
BC	1358.51	1	1358.51	0.20	0.6614	
A^2	16767.33	1	16767.33	2.51	0.1439	
B^2	1.93×10^5	1	1.93×10^5	28.93	0.0003	
C^2	36748.19	1	36748.19	5.51	0.0408	
Residual	66704.83	10	66704.83			
Lack of Fit	20404.54	5	4080.91	0.44	0.8053	not significant
Pure Error	46300.29	5	9260.06			
Corrected Total	5.93×10^5	19				

A = time of high shear; B = speed of low shear; C = sonication time

The adequacy and validity of the mathematical equations were evaluated by the regression coefficient, R^2 results for the final reduced model, and are presented in Table 5. It was found that the predicted R^2 (0.5885) was in reasonable agreement with the adjusted R^2 (0.7649), with the differences in both values being less than 0.2. If the difference between adjusted R^2 and predicted R^2 is more than 0.2, there might be a problem with either the data or the model. In addition, the adequate precision values were greater than four, and all these statistical parameters show the reliability of the models (Mousazadeh *et al*., 2014; Tan *et al*., 2016).

Response Surface Analysis

As nanoemulsion has a good spreadability and can effectively deliver the active ingredients into the skin, it is preferable to be used for cosmeceuticals properties (Rocha-Filho *et al*., 2017). Nanoemulsion enables more active ingredients to make contact with the skin via surface-to-surface interaction between the emulsion and the skin, as it creates a large surface-to-volume ratio of particles. Therefore, the minimum particle size is the main consideration in this design. Three-dimensional (3D) response surface is the graphical representation of the regression function. It was plotted to show how independent variables affect the response variables. They were presented in Figure 3 for the independent variables (time of high shear, speed of low shear and sonication time) by keeping a variable constant, which indicated the changes in particle size under two different conditions.

Table 5: Regression coefficient, R^2 results for the final reduced model

SD	81.67	**R^2**	0.8762
Mean	439.02	**Adjusted R^2**	0.7649
CV%	18.60	**Predicted R^2**	0.5885
PRESS	2.218E+005	**Adequate Precision**	7.838

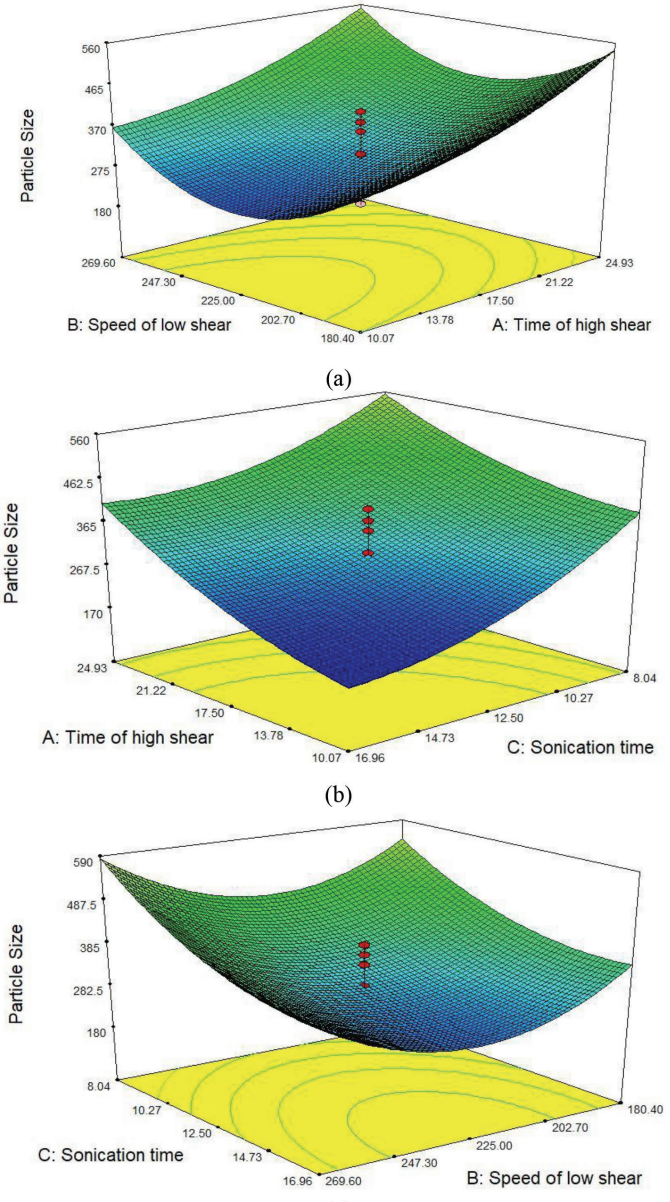

Figure 3: Response surface showing the effect of (a) time of high shear and speed of low shear; (b) time of high shear and sonication time; (c) speed of low shear and sonication time

Figure 3 shows that a longer time of high shear (A) will increase the particle size of the nanoemulsion. In high shear homogenization, the sample was forced to go through the small orifice surrounding the probe which causes the particles to break into smaller particles. With the help of a rotating impeller in the probe, high shear homogenization doubles up the process of converting the particle to a smaller size. However, in this study, a longer time of high shear results in increasing the particle size, which might be attributable to the fact that this condition promoted a higher rate of collision between the particles (Roselan *et al*., 2020). This

will promote the aggregation of small particles into larger particles, as reported by Einhorn *et al*. (2002) and Rebolleda *et al*. (2015), who observed that high shear gave the smallest particles, but exhibited rapid destabilization after a few hours. Bernardi *et al.* (2011) also stated that nanoemulsion prepared using a high-energy emulsification technique was less stable with respect to the particle size.

On the other hand, the smallest particle size was produced at a moderate speed of low shear (B). The low shear homogenization is a spontaneous method using an overhead stirrer. This low-energy emulsification technique is said to be more energy efficient which involves only a simple stirring process (Solans & Solé, 2012). The particles are subjected to no force, which will significantly break them down. However, this technique helps to homogenize and increase the spreadability of the nanoemulsion. A study by Baudonnet *et al*. (2004) discovered that increasing stirring speed decreases the particle size. As shown in Table 4, the *p*-value of the speed of low shear is 0.7209, making it insignificant in the determination of the particle size in this model. Thus, this trend might not be significant too, and modifications in the range of this parameter need to be done in further studies to give a better insight into the effect of this parameter.

As the sonication time (C) increases, the particle size significantly decreases. During sonication, the sonic waves produced by the instrument break the particles into smaller pieces. Therefore, longer sonication time can produce a smaller particle size in the production of the nanoemulsion. This was supported by Solans *et al*. (2005) who claimed that sonication was efficient in reducing particle size. Meanwhile, an experiment by Delmas *et al*. (2011) revealed that the mean diameter of the particle decreases exponentially when the sonication time increases.

Verification of Model

The verification of the final model was done to examine the adequacy of the predicted response values in the validation set. Three randomized formulations were obtained by point prediction using Design-Expert® software (version 7.1.5) to test for the sufficiency of the final model obtained. The values of the independent variables in the validation set were not found among 20 main runs, but were found in the defined range. The actual and predicted particle size of the validation set were tabulated in Table 6. The residual standard error (RSE) value was calculated to observe any significant difference between the actual and predicted particle size. The RSE values of less than 2% confirmed the adequacy of the model (Wahgiman *et al*., 2019), and the actual values were found to be quite close to the predicted values, which indicated excellent fitness of the model generated.

Optimization of the Independent Variables

Using the desirability function method in the Design-Expert® software, numerical optimization was carried out. The optimized formulation was developed based on the value of all independent variables in the range, resulting in the minimum particle size of the nanoemulsion, as shown in Table 7.

Table 6: Validation set for the verification of the final model obtained

Independent Variable			Particle Size (nm)		RSE (%)
A (min)	B (rpm)	C (min)	Actual	Predicted	
11.00	218.00	16.00	219.70	214.11	0.026
10.00	215.00	18.00	232.96	218.41	0.067
12.00	220.00	17.00	216.41	213.31	0.015

A = time of high shear; B = speed of low shear; C = sonication time

Table 7: Constraints of numerical optimization

Constraints	Goal	Lower Limit	Upper limit
Time of high shear (A)	In range	10.07	24.93
Speed of low shear (B)	In range	180.40	269.60
Sonication time (C)	In range	8.04	16.96
Particle size (nm)	Minimize	184.60	727.70

Table 8: Optimum formulation of KMO nanoemulsion

Independent Variable			Particle Size (nm)		Desirability
A (min)	B (rpm)	C (min)	Actual	Predicted	
11.16	218.32	16.75	220.41	212.54	1.00

A = time of high shear; B = speed of low shear; C = sonication time

Based on the CCD-RSM, an optimized formulation with 11.16 min (time of high shear), 218.32 rpm (speed of low shear), and 16.75 min (sonication time) was suggested, which would produce a particle size of 220.410 nm. Table 8 shows the response values of the optimized KMO nanoemulsion.

Physicochemical Characterization of KMO Nanoemulsion

Mean Particle Size, Zeta Potential and Polydispersity Index (PDI) Analysis

The mean particle size, zeta potential and polydispersity index (PDI) of the optimized nanoemulsion containing KMO were found to be 220.41 nm, −45.4 mV and 0.294, respectively. For cosmeceutical purposes, the nanoemulsion with a particle size ranging between 100 to 200 nm was more favorable (Ngan *et al*., 2014). In this study, the particle size of the KMO nanoemulsion obtained was more than 200 nm, thus further studies on the optimization of the response need to be done to obtain the desire particle size of the nanoemulsion.

The zeta potential measures the electrokinetic potential of a particle and was used to determine the stability of the nanoemulsion. A nanoemulsion with zeta potential values higher than +30 mV and lower than −30 mV was said to be stable (Ribeiro *et al*., 2015). Since the measured zeta potential of the KMO nanoemulsion was -45.4 mV, the nanoemulsion was found to be stable.

PDI value was used to analyze the uniformity of the particles in a system. The PDI value, which was near to zero, indicates a monodispersed system; meanwhile, a PDI value near to one indicates a polydispersed system (wide range of particle sizes) (Tang *et al*., 2012). Pongsumpun *et al*. (2020) stated that a nanoemulsion system is considered monodispersed (narrow size distribution) if the PDI value is less than 0.3. The optimized KMO nanoemulsion was found to be monodispersed, with the PDI value of 0.294.

pH and Conductivity Analysis

The pH of the optimized nanoemulsion containing KMO was 4.76. For topical applications, a pH in the range of 4.0 to 7.0 is preferable, as the pH of the human skin is around 5.5 (Martínez-Pla *et al*., 2004; Abd Gani *et al*., 2011). Thus, the pH of the KMO nanoemulsion was found to be in a suitable range for topical applications.

Conductivity refers to the measurement of the free amount of water and ions, as it will respond to all ions present in the solution.

This parameter helps to identify the type of nanoemulsion produced. The high conductivity value of KMO nanoemulsion, which was 1405 µS/cm, demonstrated that the aqueous phase was a continuous phase, indicating that the nanoemulsion formed was oil-in-water nanoemulsion (O/W) (Jiang *et al*., 2013). In the cosmetics industry, the O/W formulation is more favorable as it is less greasy after application.

Stability Study

Stability is one of the important parameters for nanoemulsion. A nanoemulsion should remain physically stable throughout its shelf life with no or minimal changes in the particle size. The creaming or sedimentation (phase separation) rate of the optimized nanoemulsion (in terms of shelf life) can be determined by a centrifugation test, as the centrifugation force is equivalent to the gravitational force (Mat Hadzir *et al*., 2013). The KMO nanoemulsion showed no physical changes or phase separation after being subjected to a 4000 rpm centrifugation force for 15 minutes.

A storage stability study was carried out by stored KMO nanoemulsion at three different temperatures (4, 25 and 45°C) for 90 days. Table 9 showed that the KMO nanoemulsion remained a homogenous mixture and no physical or phase changes after 90 days under all storage temperatures. Thus, the KMO nanoemulsion formed in this preliminary study was considered as stable within three months.

Conclusion

The molecular docking study revealed some variation of affinity value (-5.6 to -4.0 kcal/mol), which can be considered as potent anti-tyrosinase activity against tyrosinase enzymes. In the present study, we demonstrated the possible interactions between co-crystallised KA (from 5M8M) and KMO through hydrogen bonding, van der Waals, π-π stacked, π-alkyl, π-sigma as well as amide-π stacked interactions with several amino acid residues at the active site. Furthermore, this research indicates that the preliminary optimization of the processing parameters for the production of KMO nanoemulsion using CCD-RSM is an excellent approach in investigating the effects of time of high shear, speed of low shear, and sonication time towards the particle size as its response. Analysis of variance (ANOVA) demonstrated the fitness of model with *F*-value (7.87), *p*-value (0.0017) with non-significant lack-of-fit with a high coefficient of determination R^2=0.8762. The model was further verified with some random formulations with different conditions. The optimized conditions for the formulation of KMO nanoemulsion were 11.16 min (time of high shear), 218.32 rpm (speed of low shear), and 16.75 min (sonication time) that resulted in 220.41 nm of particle size. The physicochemical characterization showed that the KMO nanoemulsion produced was in nano-sized range, but it needs to be further optimized so that it will be suitable for cosmeceuticals use, with a zeta potential of -45.4 mV and PDI of 0.294, indicating nanoemulsion produced was stable and monodisperse. The pH of optimized nanoemulsion was 4.76, which makes it compatible with skin pH (4.0-7.0) and its conductivity was high (1405 µS/cm), indicating that the optimized nanoemulsion produced was oil-in-water nanoemulsion. The optimized nanoemulsion containing KMO remained stable

Table 9: Physical stability of KMO nanoemulsion under different storage temperature and centrifugation test

Storage Temperature (°C)	Storage Stability (days)				Centrifugation
	1	30	60	90	
4	/	/	/	/	/
25	/	/	/	/	
45	/	/	/	/	

/ = stable or no physical changes

(no phase separation was observed) under centrifugation test and accelerated stability during storage at 4°C, 25°C and 45°C within 90 days. The data from the molecular docking can be used to provide additional information on the capability of KMO as a tyrosinase inhibitor, meanwhile the preliminary optimization of the KMO nanoemulsion provides informative data that can be used to further optimize the KMO nanoemulsion with desirable criteria for the cosmeceuticals field.

Acknowledgements

This research has been funded by the Universiti Putra Malaysia under grant number 9628900. Muhammad Azimuddin Roselan and Norzalina Zakaria extend their gratitude to the university.

References

Abd Gani, S. S., Basri, M., Abdul Rahman, M. B., Kassim, A., Raja Abd Rahman, R. N. Z., Salleh, A. B., & Ismail, Z. (2011). Engkabang fat as a base in preparing encapsulated titanium dioxide for cosmetics purpose. *Asian Journal of Chemistry*, *23*(1), 380-384.

Abdellatif, A. A., & Abou-Taleb, H. A. (2015). Optimization of nano-emulsion formulations for certain emollient effect. *World Journal of Pharmacy and Pharmaceutical Sciences*, *4*(12), 1314-1328.

Al-Edresi, S., & Baie, S. (2009). Formulation and stability of whitening VCO-in-water nano-cream. *International Journal of Pharmaceutics*, *373*(1-2), 174-178. https://doi.org/10.1016/j.ijpharm.2009.02.011

Azhar, S. N. A. S., Ashari, S. E., & Salim, N. (2018). Development of a kojic monooleate-enriched oil-in-water nanoemulsion as a potential carrier for hyperpigmentation treatment. *International Journal of Nanomedicine*, *13*, 6465.

Bahari, A. N., Saari, N., Salim, N., & Ashari, S. E. (2020). Response Factorial Design Analysis on Papain-Generated Hydrolysates from Actinopyga lecanora for Determination of Antioxidant and Antityrosinase Activities. *Molecules*, *25*(11), 2663. https://doi.org/https://doi.org/10.3390/molecules25112663

Baş, D., & Boyacı, İ. H. (2007). Modeling and optimization I: Usability of response surface methodology. *Journal of Food Engineering*, *78*(3), 836-845. https://doi.org/10.1016/j.jfoodeng.2005.11.024

Baudonnet, L., Grossiord, J. L., & Rodriguez, F. (2004). Effect of dispersion stirring speed on the particle size distribution and rheological properties of three carbomers. *Journal of Dispersion Science and Technology*, *25*(2), 183-192. https://doi.org/10.1081/DIS-120030665

Bernardi, D. S., Pereira, T. A., Maciel, N. R., Bortoloto, J., Viera, G. S., Oliveira, G. C., & Rocha-Filho, P. A. (2011). Formation and stability of oil-in-water nanoemulsions containing rice bran oil: In vitro and in vivo assessments. *Journal of Nanobiotechnology*, *9*, 1-9. https://doi.org/10.1186/1477-3155-9-44

Damayanti, S., Mahardhika, A. B., Ibrahim, S., Chong, W. L., Lee, V. S., & Tjahjono, D. H. (2014). O-desmethylquinine as a cyclooxygenase-2 (COX-2) inhibitors using AutoDock Vina (Vol. 1621, pp. 103-107). https://doi.org/10.1063/1.4898452

De Azevedo Ribeiro, R. C., Barreto, S. M. A. G., Ostrosky, E. A., Da Rocha-Filho, P. A., Veríssimo, L. M., & Ferrari, M. (2015). Production and characterization of cosmetic nanoemulsions containing Opuntia ficus-indica (L.) Mill extract as moisturizing agent. *Molecules*, *20*(2), 2492-2509. https://doi.org/10.3390/molecules20022492

Delmas, T., Piraux, H., Couffin, A. C., Texier, I., Vinet, F., Poulin, P., … Bibette, J. (2011). How to prepare and stabilize very small nanoemulsions. *Langmuir*, *27*(5), 1683-1692. https://doi.org/10.1021/la104221q

Dundas, J., Ouyang, Z., Tseng, J., Binkowski, A., Turpaz, Y., & Liang, J. (2006). CASTp: Computed atlas of surface topography of

proteins with structural and topographical mapping of functionally annotated residues. *Nucleic Acids Research*, *34*(WEB. SERV. ISS.), 116-118. https://doi.org/10.1093/nar/gkl282

Einhorn-Stoll, U., Weiss, M., & Kunzek, H. (2002). Influence of the emulsion components and preparation method on the laboratory-scale preparation of o / w emulsions containing different types of dispersed phases and / or emulsifiers, *46*(4), 294-301.

Faujan, N. H., Zakaria, N., & Mohammad, N. N. (2019). Molecular docking studies on the interaction of anti-alzheimer compounds with Amyloid Beta Peptides, *6*(12), 132-136.

Forli, S., Huey, R., Pique, M. E., Sanner, M., Goodsell, D. S., & Arthur, J. (2016). Computational protein-ligand docking and virtual drug screening with the AutoDock suite. *Nature Protocols*, *11*(5), 905-919. https://doi.org/10.1038/nprot.2016.051. Computational

Fukumoto, S., Morishita, A., Furutachi, K., Terashima, T., Nakayama, T., & Yokogoshi, H. (2008). Effect of flavour components in lemon essential oil on physical or psychological stress. *Stress and Health*, *24*(1), 3-12. https://doi.org/10.1002/smi.1158

Gallarate, M., Carlotti, M. E., Trotta, M., Grande, a E., & Talarico, C. (2004). Photostability of naturally occurring whitening agents in cosmetic microemulsions. *Journal of Cosmetic Science*, *55*(2), 139-148. http://www.ncbi.nlm.nih.gov/pubmed/15131725

Heo, S. J., Ko, S. C., Kang, S. M., Cha, S. H., Lee, S. H., Kang, D. H., … Jeon, Y. J. (2010). Inhibitory effect of diphlorethohydroxycarmalol on melanogenesis and its protective effect against UV-B radiation-induced cell damage. *Food and Chemical Toxicology*, *48*(5), 1355-1361. https://doi.org/10.1016/j.fct.2010.03.001

Huang, H.-P., Shih, Y.-W., Chang, Y.-C., Hung, C.-N., & Wang, C.-J. (2008). Chemoinhibitory effect of Mulberry Anthocyanins on Melanoma Metastasis involved in the Ras/PI3K pathway. *Journal of Agricultural and Food Chemistry*, *56*(19), 9286-9293. https://doi.org/10.1021/jf8013102

Ibrahim, Z., Tejo, B. A., Mohammad Latif, M. A., Karjiban, R. A., Salleh, A. B., & Abdul Rahman, M. B. (2016). In-Silico Identification of Potential Protein Arginine Deiminase Iv (Pad4) Inhibitors. *Malaysian Journal of Analytical Science*, *20*(6), 1269-1277. https://doi.org/10.17576/mjas-2016-2006-05

Ismaya, W. T., Rozeboom, J., Weijn, A., Mes, J. J., & Fusetti, F. (2011). Crystal structure of Agaricus bisporus Tyrosinase. *Biochemistry*, *50*, 5477-5486.

Jacobus Berlitz, S., De Villa, D., Maschmann Inácio, L. A., Davies, S., Zatta, K. C., Guterres, S. S., & Külkamp-Guerreiro, I. C. (2019). Azelaic acid-loaded nanoemulsion with hyaluronic acid-a new strategy to treat hyperpigmentary skin disorders. *Drug Development and Industrial Pharmacy*, *45*(4), 642-650. https://doi.org/10.1080/03639045.2019.1569032

Jiang, J., Mei, Z., Xu, J., & Sun, D. (2013). Effect of inorganic electrolytes on the formation and the stability of water-in-oil (W/O) emulsions. *Colloids and Surfaces A: Physicochemical and Engineering Aspects*, *429*, 82-90. https://doi.org/10.1016/j.colsurfa.2013.03.039

Jumbri, K., Al-Haniff Rozy, M. F., Ashari, S. E., Mohamad, R., Basri, M., & Fard Masoumi, H. R. (2015). Optimisation and characterisation of lipase catalysed synthesis of a kojic monooleate ester in a solvent-free system by response surface methodology. *PLoS ONE*, *10*(12), 1-13. https://doi.org/10.1371/journal.pone.0144664

Kanlayavattanakul, M., & Lourith, N. (2018). Skin hyperpigmentation treatment using

herbs: A review of clinical evidences. *Journal of Cosmetic and Laser Therapy*, *20*(2), 123-131. https://doi.org/10.1080/14764172.2017.1368666

Lai, X., Wichers, H. J., Soler-Lopez, M., & Dijkstra, B. W. (2017). Structure of Human Tyrosinase Related Protein 1 Reveals a Binuclear Zinc Active Site Important for Melanogenesis. *Angewandte Chemie - International Edition*, *56*(33), 9812-9815. https://doi.org/10.1002/anie.201704616

Lohani, A., Verma, A., Joshi, H., Yadav, N., & Karki, N. (2014). Nanotechnology-based cosmeceuticals. *ISRN Dermatology*, *2014*, 1-14. https://doi.org/10.1155/2014/843687

Makeneni, S., Thieker, D. F., & Woods, R. J. (2018). Applying pose clustering and MD simulations to eliminate false positives in molecular docking. *Journal of Chemical Information and Modeling*, *58*(3), 605-614. https://doi.org/10.1021/acs.jcim.7b00588

Martínez-Pla, J. J., Martín-Biosca, Y., Sagrado, S., Villanueva-Camañas, R. M., & Medina-Hernández, M. J. (2004). Evaluation of the pH effect of formulations on the skin permeability of drugs by biopartitioning micellar chromatography. *Journal of Chromatography A*, *1047*(2), 255-262. https://doi.org/10.1016/j.chroma.2004.07.011

Mat Hadzir, N., Basri, M., Abdul Rahman, M. B., Salleh, A. B., Raja Abdul Rahman, R. N. Z., & Basri, H. (2013). Phase behaviour and formation of Fatty Acid Esters Nanoemulsions containing Piroxicam. *AAPS PharmSciTech*, *14*(1), 456-463. https://doi.org/10.1208/s12249-013-9929-1

McClements, D. J. (2011). Edible nanoemulsions: Fabrication, properties, and functional performance. *Soft Matter*, *7*(6), 2297-2316.

Mohd, A., Adnan, M. H. L., Baba, N. B., Selamat, Z. A., Rose, A. N. M., & Mohamed, S. B. (2020). Optimization of surface roughness and tool wear on AISI 4140 using coated Ni-YSZ for CNC turning process. *Journal of Physics: Conference Series*, *1532*(1). https://doi.org/10.1088/1742-6596/1532/1/012001

Mousazadeh, M., Mousavi, M., Emam-Djomeh, Z., Hadinezhad, M., & Gharibzahedi, S. M. T. (2014). Formulation optimization of pistachio oil spreads by characterization of the instrumental textural attributes. *International Journal of Food Properties*, *17*(6), 1355-1368. https://doi.org/10.1080/10942912.2012.700537

Ngan, C. L., Basri, M., Lye, F. F., Fard Masoumi, H. R., Tripathy, M., Abedi Karjiban, R., & Abdul-Malek, E. (2014). Comparison of Box-Behnken and central composite designs in optimization of fullerene loaded palm-based nano-emulsions for cosmeceutical application. *Industrial Crops and Products*, *59*, 309-317. https://doi.org/10.1016/j.indcrop.2014.05.042

Noh, J. M., Kwak, S. Y., Seo, H. S., Seo, J. H., Kim, B. G., & Lee, Y. S. (2009). Kojic acid-amino acid conjugates as tyrosinase inhibitors. *Bioorganic and Medicinal Chemistry Letters*, *19*(19), 5586-5589. https://doi.org/10.1016/j.bmcl.2009.08.041

Nostro, A., Cannatelli, M. A., Morelli, I., Musolino, A. D., Scuderi, F., Pizzimenti, F., & Alonzo, V. (2004). Efficiency of Calamintha officinalis essential oil as preservative in two topical product types. *Journal of Applied Microbiology*, *97*(2), 395-401. https://doi.org/10.1111/j.1365-2672.2004.02319.x

Panich, U., Kongtaphan, K., Onkoksoong, T., Jaemsak, K., Phadungrakwittaya, R., Thaworn, A., … Wongkajornsilp, A. (2010). Modulation of antioxidant defense by Alpinia galanga and Curcuma aromatica extracts correlates with their inhibition of UVA-induced melanogenesis. *Cell Biology and Toxicology*, *26*(2), 103-116. https://doi.org/10.1007/s10565-009-9121-2

Pey, C. M., Maestro, A., Solé, I., González, C., Solans, C., & Gutiérrez, J. M. (2006). Optimization of nano-emulsions prepared

by low-energy emulsification methods at constant temperature using a factorial design study. *Colloids and Surfaces A: Physicochemical and Engineering Aspects*, *288*(1-3), 144-150. https://doi.org/10.1016/j.colsurfa.2006.02.026

Pongsumpun, P., Iwamoto, S., & Siripatrawan, U. (2020). Response surface methodology for optimization of cinnamon essential oil nanoemulsion with improved stability and antifungal activity. *Ultrasonics Sonochemistry*, *60*(May 2019), 104604. https://doi.org/10.1016/j.ultsonch.2019.05.021

Rebolleda, S., Sanz, M. T., Benito, J. M., Beltrán, S., Escudero, I., & González San-José, M. L. (2015). Formulation and characterisation of wheat bran oil-in-water nanoemulsions. *Food Chemistry*, *167*, 16-23. https://doi.org/10.1016/j.foodchem.2014.06.097

Rocha-Filho, P. A., Ferrari, M., Maruno, M., Souza, O., & Gumiero, V. (2017). In Vitro and In Vivo evaluation of Nanoemulsion containing vegetable extracts. *Cosmetics*, *4*(3). https://doi.org/10.3390/cosmetics4030032

Roselan, M. A., Ashari, S. E., Faujan, N. H., Mohd Faudzi, S. M., & Mohamad, R. (2020). An improved Nanoemulsion formulation containing Kojic Monooleate: Optimization, characterization and In Vitro studies. *Molecules*, *25*(11), 2616.

Sanner, M. F. (1999). Python: A programming language for software integration and development. *Journal of Molecular Graphics and Modelling*, *17*(1), 57-61.

Sharma, N., Bansal, M., Visht, S., Sharma, P., & Kulkarni, G. (2010). Nanoemulsion: A new concept of delivery system. *Chronicles of Young Scientists*, *1*(2), 2-6. http://www.cysonline.org/article.asp?issn=2229-5186;year=2010;volume=1;issue=2;spage=2;epage=6;aulast=Sharma

Solans, C., Izquierdo, P., Nolla, J., Azemar, N., & Garcia-Celma, M. J. (2005). Nano-emulsions. *Current Opinion in Colloid & Interface Science*, *10*(3), 102-110.

Solans, C., & Solé, I. (2012). Nano-emulsions: Formation by low-energy methods. *Current Opinion in Colloid and Interface Science*, *17*(5), 246-254. https://doi.org/10.1016/j.cocis.2012.07.003

Solè, I., Maestro, A., Pey, C. M., González, C., Solans, C., & Gutiérrez, J. M. (2006). Nano-emulsions preparation by low energy methods in an ionic surfactant system. *Colloids and Surfaces A: Physicochemical and Engineering Aspects*, *288*(1), 138-143.

Tadros, T., Izquierdo, P., Esquena, J., & Solans, C. (2004). Formation and stability of nano-emulsions. *Advances in Colloid and Interface Science*, *108-109*, 303-318. https://doi.org/10.1016/j.cis.2003.10.023

Tan, S. F., Masoumi, H. R. F., Karjiban, R. A., Stanslas, J., Kirby, B. P., Basri, M., & Basri, H. Bin. (2016). Ultrasonic emulsification of parenteral valproic acid-loaded nanoemulsion with response surface methodology and evaluation of its stability. *Ultrasonics Sonochemistry*, *29*, 299-308. https://doi.org/10.1016/j.ultsonch.2015.09.015

Tang, S. Y., Manickam, S., Wei, T. K., & Nashiru, B. (2012). Formulation development and optimization of a novel Cremophore EL-based nanoemulsion using ultrasound cavitation. *Ultrasonics Sonochemistry*, *19*(2), 330-345. https://doi.org/10.1016/j.ultsonch.2011.07.001

Tofani, R. P., Sumirtapura, Y. C., & Darijanto, S. T. (2016). Formulation, characterisation, and in vitro skin diffusion of nanostructured lipid carriers for deoxyarbutin compared to a nanoemulsion and conventional cream. *Scientia Pharmaceutica*, *84*(4), 634-645. https://doi.org/10.3390/scipharm84040634

Trott, O., & Olson, A. J. (2009). AutoDock Vina: Improving the speed and accuracy of docking with a new scoring function, efficient optimization, and multithreading.

Journal of Computational Chemistry, *8*(8). https://doi.org/10.1002/jcc.21334

Wahgiman, N. A., Salim, N., Rahman, M. B. A., & Ashari, S. E. (2019). Optimization of nanoemulsion containing gemcitabine and evaluation of its cytotoxicity towards human fetal lung fibroblast (MRC5) and human lung carcinoma (A549) cells. *International Journal of Nanomedicine*, *14*, 7323-7338. https://doi.org/10.2147/IJN.S212635